

## Tuning the magnetic anisotropy in artificially layered $\text{Mn}_3\text{Ga}/\text{Mn}_3\text{GaN}$ superlattices

Lu Guo,<sup>1,\*</sup> Neil Campbell,<sup>2,\*</sup> Alexander J. Grutter,<sup>3</sup> Gahee Noh,<sup>5</sup> Tianxiang Nan,<sup>1</sup> P. Quarterman,<sup>3</sup> Si-Young Choi,<sup>5,6</sup> Thomas Tybell,<sup>4</sup> Mark S. Rzchowski,<sup>2</sup> and Chang-Beom Eom<sup>1,†</sup>

<sup>1</sup>*Department of Materials Science and Engineering, University of Wisconsin-Madison, Madison, Wisconsin 53706, USA*

<sup>2</sup>*Department of Physics, University of Wisconsin-Madison, Madison, Wisconsin 53706, USA*

<sup>3</sup>*NIST Center for Neutron Research, National Institute of Standards and Technology, Gaithersburg, Maryland 20899, USA*

<sup>4</sup>*Department of Electronic Systems, Norwegian University of Science and Technology, Trondheim 7491, Norway*

<sup>5</sup>*Department of Materials Science and Engineering, Pohang University of Science and Technology, Pohang 37673, Republic of Korea*

<sup>6</sup>*Center for Van der Waals Quantum Solids, Institute for Basic Science, Pohang 37673, Republic of Korea*



(Received 14 August 2023; accepted 13 October 2023; published 31 January 2024)

Artificially layered superlattices with two distinct spin structures offer new opportunities for manipulation of magnetic properties and interfacial spin configurations. We have grown epitaxial, coherent superlattices of ferrimagnetic  $\text{Mn}_3\text{Ga}$  and noncollinear antiferromagnetic  $\text{Mn}_3\text{GaN}$ . The out-of-plane ferrimagnetism of the  $\text{Mn}_3\text{Ga}$  layer, and the Berry-phase charge to spin current generation by the noncollinear antiferromagnetic  $\text{Mn}_3\text{GaN}$  layer, provide a unique combination for spintronic applications. Reactive magnetron sputtering growth resulted in abrupt transitions between the two layers through controlling the  $\text{N}_2$  flow. X-ray diffraction and cross-sectional scanning transmission electron microscopy images demonstrate clean layering and consistent modulation wavelengths, with interfacial roughness less than one unit cell. This allows investigation of the interfacial magnetic interactions. Through a combination of superconducting quantum interference device magnetometry and polarized neutron reflectometry we show that  $\text{Mn}_3\text{Ga}/\text{Mn}_3\text{GaN}$  superlattice structures have the out-of-plane magnetic anisotropy decreased compared to  $\text{Mn}_3\text{Ga}$  single-layer films. This softening is primarily a result of reduced anisotropy energy at the interface and is linked to the  $\text{Mn}_3\text{GaN}$  layer. This superlattice structure provides a platform for devices that use out-of-plane spin torques generated from an antiferromagnetic material to switch the net magnetic moment of a ferrimagnetic material. Our results demonstrate the tunability of magnetic anisotropy to allow for optimal balancing of the switching power and thermal stability in spintronic heterostructures.

DOI: [10.1103/PhysRevMaterials.8.L011401](https://doi.org/10.1103/PhysRevMaterials.8.L011401)

**Introduction.** Spin-torque devices rely on spin current generation in one material injected into another to manipulate the magnetization. As spin current can decay on short length scales, bilayer geometries optimize the functionality of such devices, with spacer layers shown to increase the interface transparency [1], increasing spin accumulation in the magnetic layer. In general, this accumulation can be optimized by increasing the interface area and by increasing the interface transparency. The first can be accomplished by increasing the interface number via artificially layered superlatticing. The second can be accomplished with coherent epitaxial heterostructures, for instance layering the  $D0_{22}$  ferrimagnet  $\text{Mn}_3\text{Ga}$  (MG) with the cubic antiperovskite  $\text{Mn}_3\text{GaN}$  (MGN) [2].

Tetragonal  $D0_{22}$  MG is a promising spintronics material due to its low saturation magnetization, high spin polarization, and strong perpendicular magnetic anisotropy [3–8]. In this  $X_2YZ$  form of Heusler materials, Mn occupies both the  $X$  and  $Y$  sites while they retain their distinct crystallographic symmetries. These different Mn sites (Mn1 and Mn2)

are antiferromagnetically aligned with different magnetic moments, resulting in a ferrimagnetic metal with out-of-plane magnetic anisotropy estimated to be in the range  $0.1 \text{ MJ/m}^3$ – $1.0 \text{ MJ/m}^3$  [5,6]. MG has metallic conductivity, with room-temperature resistivity  $100 \mu\Omega \text{ cm}$ . To incorporate MG in spintronic devices, heterostructuring with other materials is necessary. Previous attempts, using Cr and Mo layers, did not produce films with appropriate magnetic properties, likely due to strain [9,10]. We demonstrate that thin-film  $\text{Mn}_3\text{GaN}$  is an ideal heterostructuring layer for intrinsic MG thin films.

Cubic antiperovskite MGN is a promising spintronic material due to its noncollinear antiferromagnetism, close phase proximity to topological Hall effect states, and ability to generate unconventional spin-current polarizations and spin-orbit torques [11–17]. At room temperature, thin-film MGN is antiferromagnetic with  $\Gamma^{5g}$  magnetic structure [11]. This magnetic structure has been shown to produce spin currents that exert torque on out-of-plane magnetizations, such as those stabilized in MG. Strong covalent bonding and several bands at the Fermi surface lead to metallic conductivity in MGN, with room-temperature resistivity  $200 \mu\Omega \text{ cm}$  [15,18].

As MG and MGN share the same cations and cation ratio, only the body-center nitrogen differentiates the materials. As

\*These authors contributed equally to this work.

†Corresponding author: eom@engr.wisc.edu

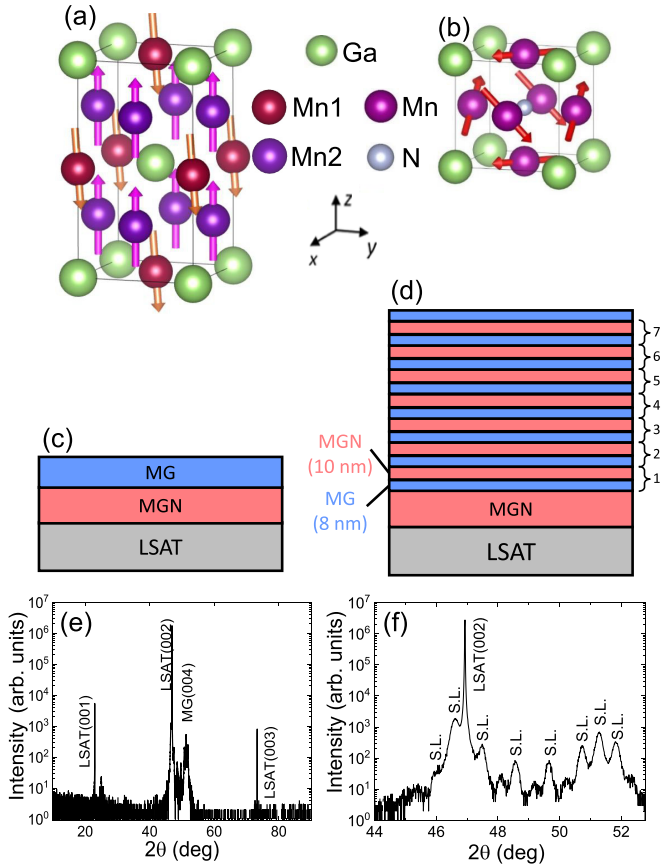


FIG. 1. The unit cells of (a)  $\text{Mn}_3\text{Ga}$  (MG) and (b)  $\text{Mn}_3\text{GaN}$  (MGN). The arrows in the figure indicate the spin directions held by corresponding Mn atoms. MG has two distinct Mn sites with different symmetries and different magnetic moment directions, Mn1 (ruby) is the minority site, and Mn2 (purple) is the majority site. MG was stabilized in (c) bilayer structures, in which a thick MGN layer provided a template for the MGN, and (d) superlattice structures, sample A, in which MGN was also used as a base layer and MG was used as a capping layer. The (e) x-ray  $\theta$ - $2\theta$  scan shows only substrate and films peaks, while the (f) highlighted region around the LSAT(002) peak of the  $\text{Mn}_3\text{Ga}/\text{Mn}_3\text{GaN}$  (MG/MGN) superlattice sample shows annotated superlattice reflections.

shown in Figs. 1(a) and 1(b), the basal planes of both unit cells have the same structure in the [001] orientation, and the next atomic layer differs only by the presence or absence of the nitrogen anion. The bulk in-plane lattice constant of MG is  $3.90 \text{ \AA}$ , while that of our thin-film MGN is  $3.91 \text{ \AA}$ , only a 0.2% difference [19]. These factors combine to allow high-quality superlattices of MG and MGN to be grown in a way that does not degrade either’s structural or magnetic properties.

Here, we demonstrate tuning magnetic properties of thin-film MG via artificially layered superlattice with MGN. MG has a strong out-of-plane magnetic easy axis when grown in [001]-oriented epitaxial thin films [5]. While our epitaxial MG thin films retain their quality and orientation in the superlattice, our magnetometry indicates the magnetization is more easily pulled into the plane in the superlattice films compared to single-layer MG films. Our polarized neutron reflectometry (PNR) measurements show that this weakening of the MG

anisotropy can be attributed to the MG/MGN interfaces. We discuss the possible origin and consequences of this change in anisotropy.

**Heterostructure growth.** High-quality epitaxial growth of thin-film MG has previously proven difficult due to its tendency toward three-dimensional island growth [20]. To overcome this, we first grew a thick (53 nm) MGN buffer layer directly on an  $(\text{LaAlO}_3)_{0.3}(\text{Sr}_2\text{TaAlO}_6)_{0.7}$  (LSAT) (001) substrate, and subsequently grew MG directly on the buffer layer. X-ray diffraction (XRD), high-resolution scanning transmission electron microscopy (HRSTEM), and magnetometry all indicate this growth produces single-crystal MG with the  $c$  axis oriented out of plane. At room temperature, the in-plane lattice constants of MG are  $3.904 \text{ \AA}$ , while our MGN films on LSAT are  $3.91 \text{ \AA}$ . Furthermore, MG and MGN have the same MnGa layer arrangement, making MGN an ideal template for oriented MG growth. Such a heterostructure also allows for the bottom MG interface to be the same for all layers and films.

Epitaxial bilayers [Fig. 1(c)] and superlattices [Fig. 1(d)] of MGN and MG were grown onto (001) LSAT substrates using DC reactive magnetron sputtering of a  $\text{Mn}_3\text{Ga}$  target. The base MGN layer was deposited with the substrate held at  $550 \text{ }^\circ\text{C}$  and under a 10-mTorr (1.33-Pa) mixture of 89% Ar and 11%  $\text{N}_2$ . All subsequent layers were grown at  $350 \text{ }^\circ\text{C}$  to avoid MG decomposition. MGN superlattice layers were grown using the previously described sputtering gas mixture, while MG layers were deposited with 3 mTorr (0.4 Pa) of pure Ar. Total pressure as well as  $\text{N}_2$  partial pressure were changed between superlattice layers, with deposition paused for up to 3 min of stabilization time before resuming growth. The superlattice sample consists of seven repeats of a MG/MGN bilayer grown on the MGN base layer, then capped by a final MG layer [Fig. 1(d)], the same thickness as in the superlattice portion, to avoid reaction (or oxidation) of the MGN with air.

Out-of-plane XRD of the superlattice sample shows broad MGN and MG  $c$ -axis diffraction peaks. MGN has a  $c$ -lattice parameter slightly larger than LSAT, placing its peak at  $46.6^\circ$  just below the substrate peak, while MG has a  $c$ -lattice parameter of  $7.1 \text{ \AA}$ , giving it a (004) peak at  $51.4^\circ$ . Both such peaks are overlaid with superlattice reflections, and so not indicated in Fig. 1(e). In Fig. 1(f), we index the superlattice reflections and determine the superlattice modulation length is  $17.7 \text{ nm}$ . The nominal thicknesses of MG and MGN in each superlattice repeating unit is  $8 \text{ nm}$  and  $10 \text{ nm}$ , respectively, repeated seven times. The nominal repeat unit thickness calibrated from the growth rate is consistent with the XRD measurements. Since neutrons have very different sensitivity from x rays, we can separate MGN and MG layer thicknesses from the neutron data, which we discuss in more detail later. The layer thicknesses based on neutron reflectometry are  $9.7 \text{ nm}$  of MG and  $8.5 \text{ nm}$  of MGN, as summarized in the Supplemental Material, Table I [21]. This contrasts with nominal thicknesses in that the MG layer is larger while the MGN layer is smaller. We speculate that the lack of  $\text{N}_2$  gas during MG growth led to the loss of nitrogen in the adjacent MGN layer, resulting in the neutron scattering fits yielding thinner MGN and thicker MG. To check the reproducibility of our results, we grew and measured two samples. The sample described above, and which we continue to discuss in the main

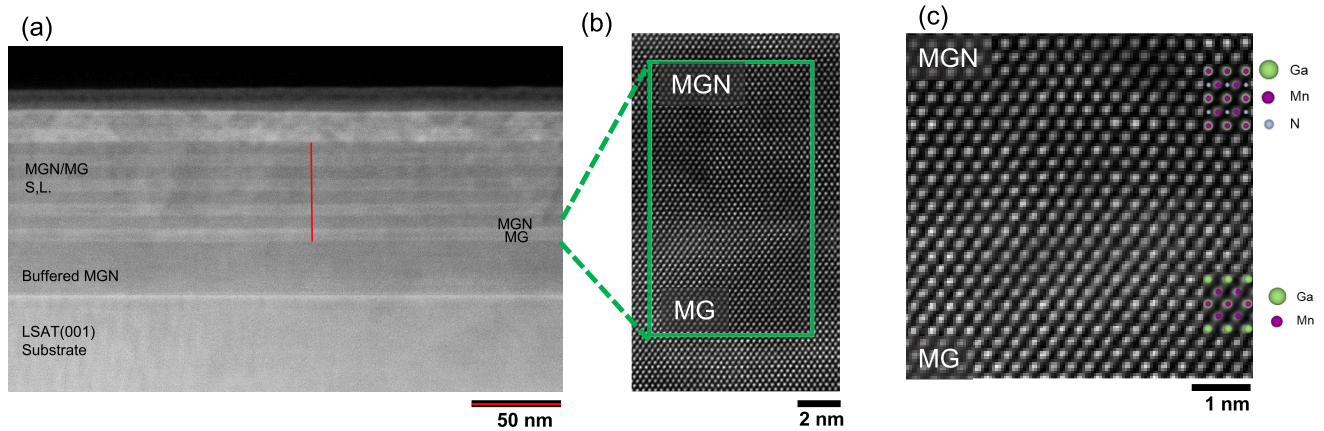


FIG. 2. (a) Low magnification STEM along the (110) zone axis shows the substrate, MGN buffer layer, and superlattice structure, with the darker layers corresponding to MGN and the lighter layers corresponding to MG. The clear contrast indicates distinct neighboring layers without serious cation interdiffusion. High-resolution STEM images show the high-quality interface between MGN and MG. (b) Adjacent MGN and MG layers are shown with no clear defects from the interface. (c) The interface between MG and MGN is coherent, and stacks of atoms are uninterrupted across the interface. To illustrate the structure, the crystal atomic structures are overlaid on the STEM image.

text, is referred to as sample A. Sample B showed the same phenomena; its data are in the Supplemental Material [21]. Bilayer MG films were grown with a similar approach where a base layer of 53 nm of MGN was deposited directly on the substrate, followed by 30 nm of MG as depicted in Fig. 1(c).

Cross-sectional STEM confirmed the layer structure and interface sharpness. The low-magnification STEM image along the [110] zone axis [Fig. 2(a)] clearly shows layered bright and dark regions from the MG and MGN layers, respectively. The contrast arises from the higher density of MG relative to MGN due to narrower out-of-plane spacing of MG yielding relatively brighter MG layers. MG and MGN cation sublattices differ in that the MnGa layer is shifted half a unit cell in the [110] direction along the  $c$  axis in MG, doubling the unit cell and enabling tighter packing. When viewed along the [110] zone axis, the MG and MGN cation lattices appear identical [Fig. 2(b)], while along the [100] zone axis the offset of the MnGa layer is apparent, as shown in the Supplemental Material, Fig. S3 [21]. These features permit interface identification to within only two MGN unit cells. STEM performed on MG/MGN superlattice samples gave layer thicknesses in good agreement with the x-ray reflectivity measurements. The higher-magnification image in Fig. 2(c) shows uninterrupted cation stacking across the interface. Such high-quality oriented growth is vital for the MG to exhibit perpendicular magnetic anisotropy over the entire sample.

**Magnetization and neutron reflectometry measurements.** To measure the perpendicular magnetic anisotropy of the MG in our samples, we used superconducting quantum interference device (SQUID) magnetometry measurements of out-of-plane magnetization versus magnetic field. The bilayer result, shown in Fig. 3(a), indicates an easy axis with a saturation magnetization of  $0.48 \mu_B/\text{Mn}$ , arising from the magnetic response of the MG layer. This value is larger than the  $0.33 \mu_B/\text{Mn}$  reported for stoichiometric MG films. Such an increase in saturation magnetization has been previously attributed to Mn deficiency, as Mn vacancies prefer minority Mn1 sites [5,6,20]. Notably, this enhancement did not impact the out-of-plane anisotropy of the MG magnetization.

We carefully determined that our superlattice sample showed a similar saturation magnetization [Fig. 3(b)]. Thus, MG in the bilayer and superlattice had similar Mn levels, allowing our measurements to probe intrinsic differences between the bilayer and superlattice samples.

Differences between bilayer and superlattice samples were apparent in the magnetic switching. This was characterized by SQUID magnetometry, measuring both in-plane and out-of-plane net moments of the films, shown in Fig. 3. The magnetization was computed per stoichiometric Mn in the MG layers according to the nominal thickness since the

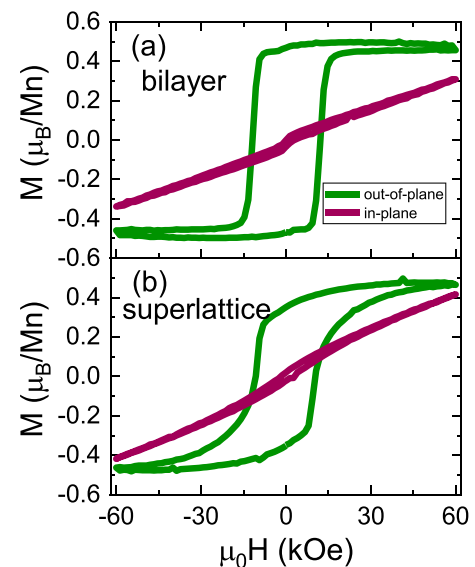


FIG. 3. Magnetization ( $M$ ) vs magnetic field ( $\mu_0 H$ ) of (a) 30-nm MG/53-nm MGN bilayer film and (b) our superlattice film, sample A, with nominal thickness information of 8-nm MG cap layer/(10-nm MGN/8-nm MGN) $_{\times 7}$ /53-nm MGN. Out-of-plane orientations are shown in green, and in-plane orientations are shown in red. All Mn used for the  $M$  units refer only to the nominal Mn in MG, not MGN since the MG provides the dominant net moment.

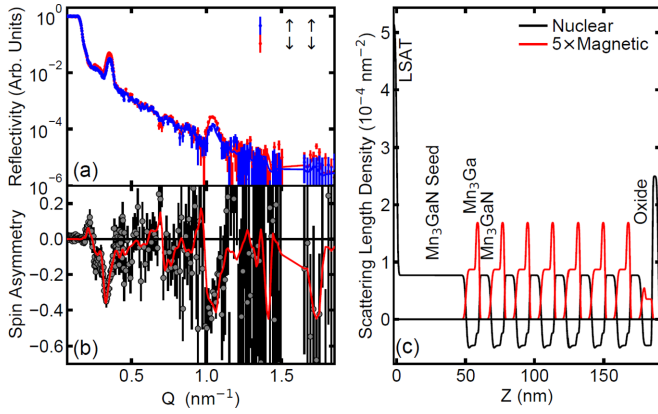


FIG. 4. Polarized neutron reflectometry (PNR) results for sample A. (a), (b) The nuclear reflectivity (a) and spin asymmetry profile (b) vs scattering vector at RT under a 3-T in-plane magnetic field of the superlattice. The solid red line is the fit and gray dots with black error bars show the experimental data. The SLD real-space profiles are shown in (c). The black line shows the nuclear SLD that is indicative of the stoichiometry of the layer, while the red line shows magnetic SLD, which is proportional to the net in-plane magnetic moment. Error bars represent  $\pm 1$  standard deviation.

MGN is antiferromagnetic with insignificant magnetization. Both samples showed similar out-of-plane coercive fields of approximately 1.2 T, and similar saturation magnetizations around  $0.48 \mu_B/\text{Mn}$ . The bilayer film's out-of-plane hysteresis loop was close to square, indicative of a strong out-of-plane easy axis anisotropy. This contrasted with the superlattice sample which showed significantly more curvature through the switching, indicative of a portion of the magnetization rotating in plane at zero field due to a weaker out-of-plane anisotropy. The in-plane magnetization curves for both films support this interpretation, as the bilayer sample showed near-ideal hard-axis character, while the superlattice shows a nonlinear contribution at fields below 3 T. Thus, with in-plane field, at 3 T the superlattice sample has more in-plane magnetization than the bilayer sample. We determined from the in-plane magnetization measurements an out-of-plane anisotropy energy density of  $1.2 \text{ MJ/m}^3$  for the bilayer in good agreement with Rode *et al.* and  $0.85 \text{ MJ/m}^3$  for the superlattice [5]. This value is roughly 40 times larger than the thin-film demagnetizing energy density, indicating that this change in anisotropy is intrinsic to the MG. The similarity in the out-of-plane coercive fields between the bilayer and superlattice samples suggests that only a portion of the MG layers is subject to the reduced anisotropy.

To check this, we studied the in-plane magnetization in the superlattices by performing room-temperature PNR measurements. PNR senses only the net in-plane magnetization, through the spin-dependent neutron reflectivities. We applied a 3-T in-plane field for all measurements to partially rotate the magnetization in plane. Incident and scattered neutrons were spin polarized either parallel or antiparallel to this applied in-plane field. We focus on the non-spin-flip reflectivities ( $R^{\uparrow\uparrow}$  and  $R^{\downarrow\downarrow}$ ) [red and blue data of Fig. 4(a)] in which the incident and scattered neutrons possess the same spin direction. These are sensitive to the magnetization parallel to the applied

magnetic field. The spin-flip reflectivities ( $R^{\uparrow\downarrow}$  and  $R^{\downarrow\uparrow}$ ) probe the in-plane magnetization perpendicular to the applied field, which is not expected to be present.

PNR measurements were carried out on both superlattice samples, but we focus here on the results from sample A and discuss similar results from sample B in the Supplemental Material [21]. Figure 4(a) shows the spin-dependent neutron reflectivities, from which we calculated the associated spin asymmetry  $\frac{R^{\uparrow\uparrow} - R^{\downarrow\downarrow}}{R^{\uparrow\uparrow} + R^{\downarrow\downarrow}}$  [Fig. 4(b)]. We determined the nuclear and magnetic scattering length density (SLD) depth profiles [Fig. 4(c)] within the superlattice by optimizing the calculated fit to the experimental scattering vector ( $Q$ ) dependent reflectivity and spin asymmetry. The nuclear SLD indicates the elemental composition and density, while the magnetic SLD is directly proportional to the net in-plane magnetization parallel to the applied field. The horizontal axis  $Z$  is the distance from the LSAT substrate surface. More details on the measurement and fitting procedures are in the Supplemental Material.

We show reflectivity data [Figs. 4(a) and 4(b)] for  $Q$  measured up through the fifth-order superlattice Bragg reflections, and the optimal fit to the spin asymmetry signal. The depth profiles for both nuclear and magnetic SLD are shown in Fig. 4(c) and match well with our nominal superlattice structure. While we did not find it necessary to include in the depth profiles any net magnetization in the MGN layers, as expected given the antiferromagnetic order, a nonuniform magnetization profile within the MG layer is necessary to fully capture the scattering across the entire measured  $Q$  range. A simple model assuming uniform magnetization within each MG layer fails to capture the spin splitting at the second-, third-, and fifth-order superlattice reflections, as shown in the Supplemental Material [21]. Allowing for a slight increase of the nuclear SLD and an enhancement of the magnetic SLD at the upper MG/MGN interface of each bilayer results in excellent agreement with the data for sample A. As discussed in the Supplemental Material, sample B fitting pointed toward magnetic SLD enhancement at both upper and lower MG/MGN interfaces. We conclude therefore that with a 3-T applied magnetic field in plane, the net in-plane magnetization in the MG is enhanced near these interfaces. This indicates a weakened perpendicular magnetic anisotropy at the interface that allows more in-plane magnetization rotation from the applied field and is consistent with the smaller perpendicular anisotropy in the superlattices compared to the bilayer MG films determined from our magnetization measurements. Measurements on sample B, detailed in the Supplemental Material, Fig. 5, support this interpretation of weakened magnetic anisotropy at the interface with limited differences; in sample B, the fitting pointed toward magnetic SLD enhancement at both MG/MGN interfaces.

**Conclusions.** Having identified that the observed superlattice weakened anisotropy arises from the MG/MGN interface, we now speculate about its origin. The HRSTEM images showed perfect cation structure across the interface, effectively ruling out a structural effect or a Mn stoichiometry effect at the interface. Furthermore, as the bilayer indicates, the slight strain from growing MG on MGN does not change the anisotropy. In fitting the neutron reflectometry profiles, concomitant with the interfacial bump in magnetic SLD, we find an increase in the nuclear SLD. As the nuclear scattering

length of nitrogen is relatively large, a small amount of nitrogen diffused across the interface would cause this. We speculate that nitrogen is accommodated within the partial Mn octahedra in MG (five nearest-neighbor Mn atoms), corresponding to its location in MGN at the Mn octahedra centers. It is known that Mn-N-Mn exchange interactions control the MGN magnetic structure, and we argue that similar interactions are responsible for the change of the net anisotropy of the MG layer [13]. Transitioning between MGN and MG growth during superlattice synthesis could result in slightly different characteristics of the top and bottom interfaces, and potentially different nitrogen diffusion at each of them. This could quantitatively change the magnetic anisotropy at the interface.

We have successfully fabricated high-quality epitaxial MG/MGN superlattices and bilayer films with atomically smooth interfaces, in which the presence of nitrogen, an anion, in a constant cation stoichiometry controls the magnetic properties of the layers. Cross-sectional HRSTEM and XRD results confirm the correct phase and sharp interfaces. This demonstrates creation of a superlattice by altering only the gas during growth. Magnetometry measurements show a reduced anisotropy energy in the superlattices that PNR data indicate arises from the MG/MGN interface. Our observations

demonstrate that the magnetism of this MG/MGN system shows strong dependence on the bulk and surface chemistry, providing the capability to tune magnetic and spin transport properties. Our findings show a pathway to manipulate magnetism in this system with a small amount of chemical tuning, and a way to modify anisotropy characteristics for spintronic applications.

The data that support the findings of this Letter are available from the corresponding author upon reasonable request.

*Acknowledgments.* This research is funded by a Vannevar Bush Faculty Fellowship (ONR Grant No. N00014-20-1-2844), the Gordon and Betty Moore Foundation's EPiQS Initiative Grant No. GBMF9065 to C.B.E., and NSF through the University of Wisconsin MRSEC (Grant No. DMR-2309000). Magnetic measurements at the University of Wisconsin-Madison was supported by the U.S. Department of Energy, Office of Science, Office of Basic Energy Sciences, under Grant No. DE-FG02-06ER46327. STEM measurements at the Pohang University of Science and Technology were supported by a Korea Basic Science Institute (National Research Facilities and Equipment Center) grant funded by the Ministry of Education (Grant No. 2020R1A6C101A202).

The authors have no conflicts to disclose.

- 
- [1] C. H. Chen, P. Tseng, Y. Y. Yang, and W. J. Hsueh, Enhancement of thermal spin transfer torque by double-barrier magnetic tunnel junctions with a nonmagnetic metal spacer, *J. Phys. Condens. Matter* **29**, 025806 (2016).
- [2] S. C. Baek, V. P. Amin, Y.-W. Oh, G. Go, S.-J. Lee, G.-H. Lee, K.-J. Kim, M. D. Stiles, B.-G. Park, and K.-J. Lee, Spin currents and spin-orbit torques in ferromagnetic trilayers, *Nat. Mater.* **17**, 509 (2018).
- [3] H. Guo, Z. Feng, H. Yan, J. Liu, J. Zhang, X. Zhou, P. Qin, J. Cai, Z. Zeng, X. Zhang *et al.*, Giant piezospintronic effect in a noncollinear antiferromagnetic metal, *Adv. Mater.* **32**, 2002300 (2020).
- [4] H.-W. Bang, W. Yoo, C. Kim, S. Lee, J. Gu, Y. Park, K. Lee, and M.-H. Jung, Structural, magnetic, and electrical properties of collinear antiferromagnetic heteroepitaxy cubic Mn<sub>3</sub>Ga thin films, *Appl. Phys. Lett.* **115**, 012402 (2019).
- [5] K. Rode, N. Baadji, D. Betto, Y.-C. Lau, H. Kurt, M. Venkatesan, P. Stamenov, S. Sanvito, J. M. D. Coey, E. Fonda *et al.*, Site-Specific order and magnetism in tetragonal Mn<sub>3</sub>Ga thin films, *Phys. Rev. B* **87**, 184429 (2013).
- [6] J. Winterlik, B. Balke, G. H. Fecher, C. Felser, M. C. M. Alves, F. Bernardi, and J. Morais, Structural, electronic, and magnetic properties of tetragonal Mn<sub>3-x</sub>Ga: Experiments and first-principles calculations, *Phys. Rev. B* **77**, 054406 (2008).
- [7] J. C. Slonczewski, Current-driven excitation of magnetic multilayers, *J. Magn. Magn. Mater.* **159**, L1 (1996).
- [8] J. C. Slonczewski, Currents and torques in metallic magnetic multilayers, *J. Magn. Magn. Mater.* **247**, 324 (2002).
- [9] R. M. Gutiérrez-Pérez, R. López Antón, K. Załęski, J. T. Holguín-Momaca, F. Espinosa-Magaña, and S. F. Olive-Méndez, Tailoring magnetization and anisotropy of tetragonal Mn<sub>3</sub>Ga thin films by strain-induced growth and spin orbit coupling, *Intermetallics* **92**, 20 (2018).
- [10] R. M. Gutiérrez-Pérez, J. T. Holguín-Momaca, J. T. Elizalde-Galindo, F. Espinosa-Magaña, and S. F. Olive-Méndez, Giant magnetization on Mn<sub>3</sub>Ga ultra-thin films grown by magnetron sputtering on SiO<sub>2</sub>/Si(001), *J. Appl. Phys.* **117**, 123902 (2015).
- [11] T. Nan, C. X. Quintela, J. Irwin, G. Gurung, D. F. Shao, J. Gibbons, N. Campbell, K. Song, S. Y. Choi, L. Guo *et al.*, Controlling spin current polarization through non-collinear antiferromagnetism, *Nat. Commun.* **11**, 4671 (2020).
- [12] C. X. Quintela, K. Song, D.-F. Shao, L. Xie, T. Nan, T. R. Paudel, N. Campbell, X. Pan, T. Tybell, M. X. Rzhowski *et al.*, Epitaxial antiperovskite/perovskite heterostructures for materials design, *Sci. Adv.* **6**, eaba4017 (2020).
- [13] M. Mochizuki, M. Kobayashi, R. Okabe, and D. Yamamoto, Spin model for nontrivial types of magnetic order in inverse-perovskite antiferromagnets, *Phys. Rev. B* **97**, 060401(R) (2018).
- [14] O. Gomonay, Berry-Phase effects and electronic dynamics in a noncollinear antiferromagnetic texture, *Phys. Rev. B* **91**, 144421 (2015).
- [15] G. Gurung, D.-F. Shao, T. R. Paudel, and E. Y. Tsymlal, Anomalous Hall conductivity of a non-collinear magnetic antiperovskite, *Phys. Rev. Mater.* **3**, 044409 (2019).
- [16] D. Fruchart and E. F. Bertaut, Magnetic studies of the metallic perovskite-type compounds of manganese, *J. Phys. Soc. Jpn.* **44**, 781 (1978).
- [17] D. Fruchart, Ph. L'Héritier, and R. Fruchart, Transformations de phases dans les nitrures et carbures du manganèse

- de structure-type perovskite, *Mater. Res. Bull.* **15**, 415 (1980).
- [18] H. Tashiro, R. Suzuki, T. Miyawaki, K. Ueda, and H. Asano, Preparation and properties of inverse perovskite  $\text{Mn}_3\text{GaN}$  thin films and heterostructures, *J. Korean Phys. Soc.* **63**, 299 (2013).
- [19] B. Balke, G. H. Fecher, J. Winterlik, and C. Felser,  $\text{Mn}_3\text{Ga}$ , a compensated ferrimagnet with high Curie temperature and low magnetic moment for spin torque transfer applications, *Appl. Phys. Lett.* **90**, 152504 (2007).
- [20] H. Kurt, K. Rode, M. Venkatesan, P. Stamenov, and J. M. D. Coey, High spin polarization in epitaxial films of ferrimagnetic  $\text{Mn}_3\text{Ga}$ , *Phys. Rev. B* **83**, 020405(R) (2011).
- [21] See Supplemental Material at <http://link.aps.org/supplemental/10.1103/PhysRevMaterials.8.L011401> for more details about structural and magnetic characterizations of superlattice films.